Cooperative dynamics across distinct structural elements regulate PTP1B activity

Received for publication, June 1, 2020, and in revised form, July 30, 2020 Published, Papers in Press, July 31, 2020, DOI 10.1074/jbc.RA120.014652

Kristiane R. Torgeson, Michael W. Clarkson, Ganesan Senthil Kumar, Rebecca Page, and Wolfgang Peti*

From the Department of Chemistry and Biochemistry, University of Arizona, Tucson, Arizona, USA

Edited by Karen G. Fleming

Protein-tyrosine phosphatase 1B (PTP1B) is the canonical enzyme for investigating how distinct structural elements influence enzyme catalytic activity. Although it is recognized that dynamics are essential for PTP1B function, the data collected thus far have not resolved whether distinct elements are dynamically coordinated or, alternatively, whether they fulfill their respective functions independently. To answer this question, we performed a comprehensive ^{13}C-methyl relaxation study of Ile, Leu, and Val (ILV) residues of PTP1B, which, because of its substantially increased sensitivity, provides a comprehensive understanding of the influence of protein motions on different time scales for enzyme function. We discovered that PTP1B exhibits dynamics at three distinct time scales. First, it undergoes a distinctive slow motion that allows for the dynamic binding and release of its two most N-terminal helices from the catalytic core. Second, we showed that PTP1B ^{13}C-methyl group side chain fast time-scale dynamics and ^{15}N backbone fast time-scale dynamics are fully consistent, demonstrating that fast fluctuations are essential for the allosteric control of PTP1B activity. Third, and most importantly, using ^{13}C ILV constant-time Carr–Purcell–Meiboom–Gill relaxation measurements experiments, we demonstrated that all four catalytically important loops—the WPD, Q, E, and substrate-binding loops—work in dynamic unity throughout the catalytic cycle of PTP1B. Thus, these data show that PTP1B activity is not controlled by a single functional element, but instead all key elements are dynamically coordinated. Together, these data provide the first fully comprehensive picture on how the validated drug target PTP1B functions.

Protein-tyrosine phosphatase 1B (PTP1B, *PTPN1*) was the first non–receptor-bound protein-tyrosine phosphatase (PTP) isolated (1). Not surprisingly, it is also the best-studied member of the human PTP family (2). Since its discovery, PTP1B has been shown to have diverse roles in multiple cellular processes, especially glucose uptake, body mass regulation, motility, and proliferation. As a consequence, PTP1B is a validated target for multiple diseases, especially diabetes and cancer (3).

PTP1B catalyzes the hydrolysis of phosphorylated tyrosine residues (4). The catalytic site is defined by: 1) the PTP loop ((I/V)HC*XX*G*XX*R(S/T)G), which includes Cys^{215}, which functions as the catalytic nucleophile in the first step of hydrolysis; 2) the WPD loop, ^{179}WPD^{181}, which contains Asp^{181}, which functions as the proton donor and acceptor during phosphoryl transfer; 3) the E loop, which plays a role in substrate recruitment; 4) the substrate-binding loop (SBL), which restricts dephosphorylation to tyrosine residues; and 5) the Q loop (residues 261–265), which includes the key residue Gln^{262}, which is responsible for coordinating a nucleophilic water, ensuring that PTPs do not function as phosphotransferases (Fig. 1*A*) (5). Upon substrate binding, it is the WPD loop that undergoes the largest structural change, moving from an open (hydrolysis incompetent) to a closed (hydrolysis competent) position. Finally, PTP1B was also shown nearly 20 years ago to contain an allosteric binding pocket that is ~20 Å away from the catalytic site, at the intersection of helices α3, α6, and α7 (6).

Recently, a number of reports have shown that dynamics play a critical role in PTP1B enzyme activity and allostery (7–9). In addition to dynamics, these reports also highlighted the importance of structural rigidity in the extended WPD loop, particularly for proline residue Pro^{185} (7). This proline is essential for PTP1B activity because it controls an indispensable CH/π switch that associates either with Trp^{179} within the WPD loop (closed state) or Phe^{269} from helix α6 (open state; Fig. S1). This CH/π switch controls WPD motion (7, 10). Further, PTP1B helix α3 was identified as the mechanical/dynamics support that drives the transition between the open and closed states of the WPD loop and serves as the connector between the WPD loop and the allosteric pocket and helix α7 (7).

Together, these structural and dynamics data have revealed many key aspects of PTP1B activity and regulation. However, there remains a key unresolved question: whether the observed dynamics for distinct structural elements are independent of one another, or, alternatively, if their dynamics are coordinated so that all catalytically critical residues work in dynamic unity throughout the PTP1B catalytic cycle. The previously reported data were primarily based on ^{15}N-based protein backbone NMR measurements (7, 11), which are excellent reporters on many aspects of protein function. However, when working with larger proteins such as PTP1B, some of these experiments have low sensitivity, decreasing measurement accuracy and making the data statistically unreliable.

Thus, to answer this question, we used ^{13}C-methyl relaxation studies of Ile, Leu, and Val (ILV) residues in PTP1B (12–14). The fast rotation of methyl groups in ILV residues ensures that these NMR experiments have high sensitivity, allowing the dynamics of PTP1B to be determined at three distinct time scales: fast (ps/ns), intermediate (μs/ms), and slow (ms/s). Our data confirm our previous discovery (using only ^{15}N-based protein backbone NMR measurements) that fast motions are critical

This article contains supporting information.

* For correspondence: Wolfgang Peti, wolfgangpeti@email.arizona.edu.

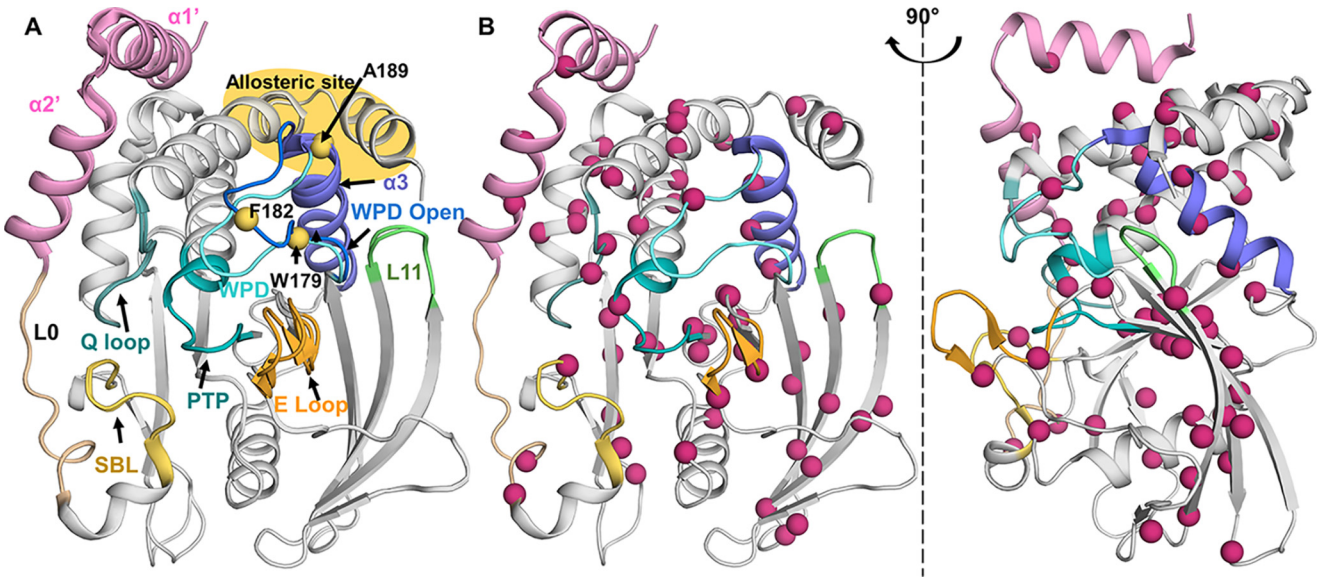

Figure 1. ^{13}C ILV methyl groups are well-dispersed throughout PTP1B. *A*, overlay of PTP1B (open state, PDB 5K9V; closed state, PDB 5K9W); active site: PTP and Q loop (*teal*), WPD loop (open, *blue*; closed, *cyan*); substrate recruitment: E and SBL loop (*yellow*/*orange*). *Purple*, helix α3; *green*, loop L11. The known allosteric site is highlighted in *yellow* at the intersection of helices α3, α6, and α7. Residues previously studied by ^{15}N ct-CPMG relaxation measurements are shown as *yellow spheres*. *B*, PTP1B (PDB 5K9W) Ile, Leu, and Val residues depicted as *pink spheres*; well-distributed throughout PTP1B.

for the regulation of allostery in PTP1B. However, we also demonstrate that intermediate time-scale motions regulate PTP1B activity. Critically, the motions observed in our ^{13}C ILV data extend far beyond the previously reported movement of the WPD loop and have revealed that PTP1B substrate recruitment and dephosphorylation function in dynamic unison. Such behavior has also been seen for other enzymes, including the enzymes dihydrofolate reductase (15, 16), cyclophilin A (17), and the kinases p38 (18) and extracellular signal–regulated kinase 2 (19). Together, this work lays the foundation for a comprehensive understanding of conformation and dynamics for the entire PTP family specifically and enzyme function and protein allostery generally.

Results

^{13}C ILV methyl assignment of PTP1B identifies reporters distributed throughout the protein

Fundamental insights into the dynamics and the function of a protein can be obtained by studying the ^{15}N backbone and/or the ^{13}C side chain dynamics, especially of Ile, Leu, and Val residues. We recently reported the ^{15}N-based sequence specific backbone assignment of the folded catalytic domain of PTP1B (~35 kDa; residues 1–301; hereafter referred to as PTP1B) and leveraged these data to define how ^{15}N fast time-scale dynamics contributes to PTP1B activity, especially allostery (20). However, the relatively large size of PTP1B, together with the inability to concentrate the protein to ≥250 μM, made ^{15}N constant-time Carr–Purcell–Meiboom–Gill (ct-CPMG) data analysis, which reports on intermediate (μs to ms) events, statistically inaccurate and thus unable to provide insights into the role of intermediate time-scale dynamics for PTP1B function. The only intermediate (μs to ms) time-scale experiments previously performed on PTP1B used three reporters (Trp^{179} and Phe^{182} in the WPD loop and Ala^{189} in helix α3; Fig. 1*A*) in free PTP1B and a single reporter (Ala^{189} in helix α3) in a peptide-bound PTP1B complex (11). These limited data suggested that intermediate time-scale motions control the WPD loop movement and subsequently its catalytic activity. However, because of the very limited number of reporters, how intermediate time-scale motions from other regions of PTP1B also contribute to its catalytic function is completely unknown. Because a few reports have recently shown that in other signaling enzymes (kinases and phosphatases) the intermediate time-scale dynamics of distinct functional regions typically work in concert for full functionality, additional studies of PTP1B that report on all functional regions are needed to understand how PTP1B intermediate time-scale dynamics control PTP1B substrate binding and activity.

PTP1B contains 60 ILV residues that are uniformly distributed throughout its sequence and structure (16 Ile, 28 Leu, and 16 Val; Fig. 1*B*). A suite of complementary experiments (21), which included NOE experiments and measurements on 16 single amino acid variants, enabled us to complete the PTP1B ^{13}C ILV methyl group assignment in both its free (Fig. S2*A*; open; 98% assigned; only Leu^{88} is missing because of overlap) and active-site inhibitor TCS-401–bound forms (Fig. S2*B*; closed; 96% assigned; Leu^{88} and Val^{49}Cδ_2 are overlapped; Ile^{219} is either broadened beyond detectability or overlapped). Our complete ILV assignment also correlates well with a partial assignment of the Ile-only region of PTP1B that was recently reported (10).

NMR ^{15}N-based sequence-specific backbone assignments of large proteins, such as PTP1B, are often incomplete because of either slow hydrogen/deuterium (H/D) back exchange after protein expression in D_2O-based medium or intermediate conformational exchange, which broadens peaks beyond detection (22). These are not issues for ^{13}C ILV methyl group assignment. Nevertheless, when counting the number of peaks in the Ile Cδ region of the spectrum, we observed 4 more peaks than

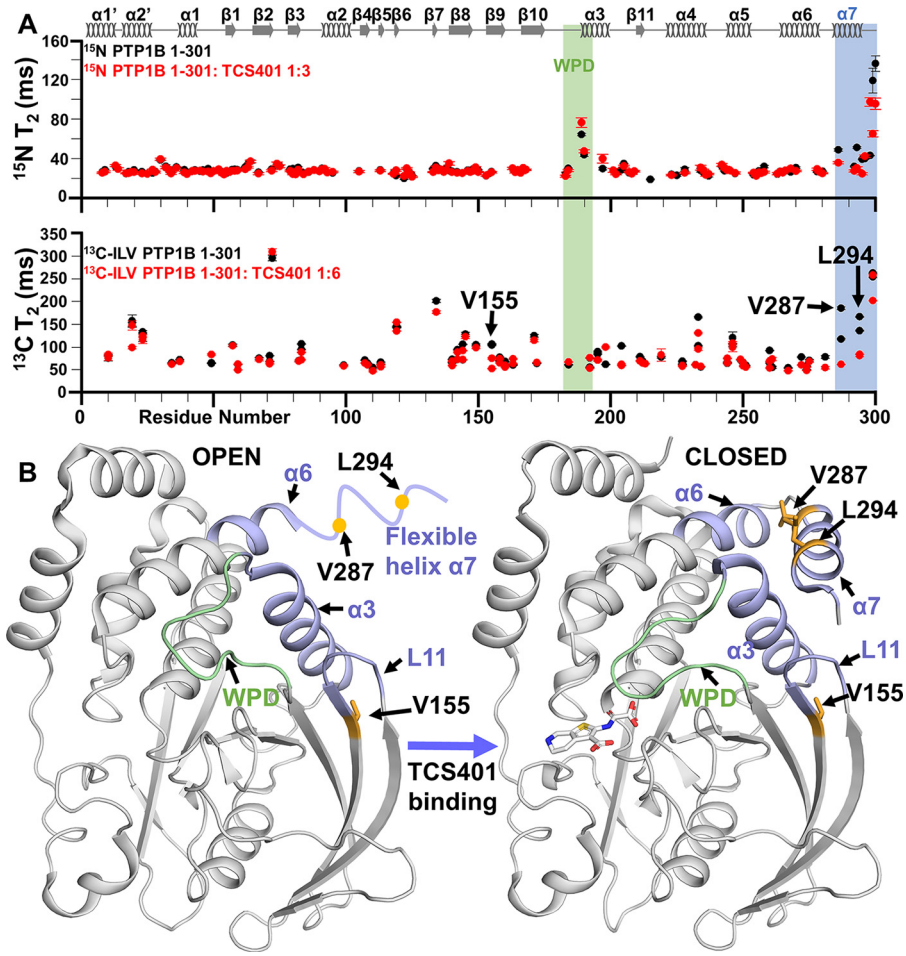

Figure 2. Change in fast time-scale ^{13}C ILV relaxation dynamics of PTP1B upon active-site interaction. *A*, ^{15}N T_2 relaxation and ^{13}C-methyl transverse T_2 rates for PTP1B (*black*) and PTP1B:TCS401 (*red*). The regions of secondary structures are illustrated at the *top* of the figure. *B*, Val^{287} and Leu^{294} (*yellow*) show a large change in dynamics as helix α7 becomes less flexible when inhibitor binds and becomes part of the allosteric site (*blue*). Val^{155} (*yellow*) interacts with key allosteric residues Tyr^{152} and Tyr^{153} to communicate to the WPD loop (*green*). The panel also shows a dramatic decrease in fast time-scale dynamics.

expected (16 expected; 20 observed; Fig. S3*A*). The assignment showed that these peaks belong to a minor conformation of Ile^{10}, Ile^{19}, Ile^{23}, and Ile^{246}, which form the interface between the catalytic PTP1B domain and helices α1′ and α2′ (Fig. S3*B*). Thus, it is likely that helices α1′ and α2′ disengage from the core protein in a slow dynamics event (p_B = ~25%), because they are only loosely connected to the catalytic domain via L0, a 10–amino acid–long linker (PTP1B residues 28–37).

PTP1B fast time-scale ^{13}C ILV relaxation data correlate with PTP1B ^{15}N backbone relaxation data

To define the PTP1B motions at different time scales, we recorded T_1 and $T_{1\rho}/T_2$ fast time scale ^{13}C ILV side-chain relaxation data (Fig. 2*A* and Fig. S4). The values of these parameters typically correlate with the distance of the ^{13}C-methyl group from the backbone, *i.e.* the further the distance, the higher the flexibility. The fast time-scale ^{13}C ILV relaxation data show this is also true for PTP1B, in which on average the methyl groups of valine residues rotate the slowest, followed by leucine and isoleucine (Fig. S5, *A* and *B*). Plotting the PTP1B T_2 ^{13}C ILV side chain relaxation data against the protein sequence and comparing it directly with our previously reported ^{15}N backbone relaxation data (T_1, T_2) show an overall similar behavior. This includes a sharp increase in overall dynamics of helix α7, which we previously established as the central modulator of allostery in PTP1B (Fig. 2, *A* and *B*). The only region in which the T_2 ^{13}C ILV side-chain and ^{15}N backbone relaxation data differ is for PTP1B helix α3, which modulates WPD motion and subsequently PTP1B activity; helix α3 did not show the increased dynamics identified in the ^{15}N backbone relaxation data (7).

^{13}C ILV assignment and side chain dynamics of closed PTP1B

Next, we determined the consequences of active-site inhibitor binding on PTP1B chemical shifts and dynamics. TCS401 is a small (306 Da) active-site inhibitor that binds PTP1B with a K_D of ~26 ± 2 μM (23). We and others have shown that the binding of small molecule inhibitors and/or substrate peptides leads to the closure of the WPD loop and a rearrangement of PTP1B helix α3, which rigidifies helix α7. As expected, direct comparison of the ^{15}N-backbone chemical shift perturbation data with that of ^{13}C ILV shows excellent overlap (Fig. S6). Notably, PTP1B helices α1′ and α2′ still disengage from the core enzyme (p_B = ~29%) in TCS401-saturated PTP1B,

Table 1
PTP1B residues: specific intermediate exchange group

k_{ex} (s^{-1})	p_B (%)	Residues
3550 ± 70	3.2 ± 0.4	Ile^{19}, Val^{49} ($C\gamma_1$ and $C\gamma_2$), Ile^{72}, Leu^{83} ($C\delta_1$ and $C\delta_2$), Val^{107} ($C\gamma_1$), Val^{113} ($C\gamma_1$ and $C\gamma_2$), Leu^{119} ($C\delta_1$ and $C\delta_2$), Ile^{134}, Leu^{142} ($C\delta_1$), Leu^{144} ($C\delta_1$ and $C\delta_2$), Val^{155} ($C\gamma_1$ and $C\gamma_2$), Leu^{160} ($C\delta_1$ and $C\delta_2$), Leu^{163} ($C\delta_1$ and $C\delta_2$), Ile^{171}, Leu^{172} ($C\delta_1$), Val^{184} ($C\gamma_1$), Leu^{195} ($C\delta_1$ and $C\delta_2$), Val^{212} ($C\gamma_1$), Ile^{219}, Leu^{227} ($C\delta_1$ and $C\delta_2$), Leu^{232} ($C\delta_1$), Leu^{233} ($C\delta_1$ and $C\delta_2$), Leu^{234} ($C\delta_1$), Val^{249} ($C\gamma_1$ and $C\gamma_2$), Leu^{250} (Cδ1 and $C\delta_2$), Leu^{260} ($C\delta_1$), Leu^{261} ($C\delta_1$), Leu^{267} ($C\delta_1$), Leu^{272} ($C\delta_1$), Val^{274} ($C\gamma_1$ and $C\gamma_2$), Leu^{275} ($C\delta_1$), Val^{287} ($C\gamma_1$), Leu^{294} ($C\delta_1$ and $C\delta_2$)
6160 ± 360	1.8 ± 1.0	Leu^{110} ($C\delta_1$ and $C\delta_2$), Leu^{140} ($C\delta_1$ and $C\delta_2$), Ile^{281}

showing that binding of TCS-401 does not influence this slow dynamics event (Fig. S3*C*).

To determine whether altered dynamics accompanies active-site inhibitor binding, we repeated the ^{13}C ILV side chain relaxation dynamics measurements with TCS401-saturated PTP1B. The most significant changes were observed in helix $\alpha7$, in which the dynamics detected in the TCS401-free state were quenched in the TCS401-saturated state. This is identical to what was observed in the ^{15}N relaxation data (R_1, R_2) that probe fast time-scale backbone dynamics (Fig. 2*A*) (7). Val^{287} and Leu^{294} show the largest changes, which define the core of the PTP1B allosteric site, at the intersection of helices $\alpha3$, $\alpha6$, and $\alpha7$ (Fig. 2*B*). Thus, these results further highlight the critical role of helix $\alpha7$ and its intrinsic dynamics for the PTP1B allosteric network. Finally, consistent with the PTP1B ^{15}N backbone relaxation data and the ^{13}C ILV chemical shift perturbation data, Val^{155} also has a statistically significant reduction in ^{13}C ILV side-chain fast time-scale dynamics (Fig. 2*A*). Val^{155} abuts the L11 loop, which includes Tyr^{152} and Tyr^{153}, two residues that are important for the allosteric pathway in PTP1B. Together, these data show that the fast time-scale dynamics results between the ^{15}N backbone relaxation and the ^{13}C ILV side chain relaxation data are consistent, a critical step before evaluating the ^{13}C ILV side-chain ct-CPMG data.

^{13}C ILV intermediate time-scale dynamics of PTP1B

Next, we measured ^{13}C ILV ct-CPMG side-chain relaxation data (all ^{13}C ILV ct-CPMG for the studies reported here are recorded at two magnetic fields; 14.1 and 18.8 T), which reports on μs-to-ms motions, for free PTP1B. Enzymatic reactions for signaling enzymes such as PTP1B often have catalytic turnover rates (PTP1B 15–60 s^{-1}) that can be correlated with protein dynamics in the μs-to-ms time scale. In ct-CPMG measurements, residues undergoing μs-to-ms conformational exchange dynamics show changes in the effective relaxation rate R_2 ($R_{2,eff}$), which are measured as a function of the repetition frequency (ν_{CPMG}). Plots of $R_{2,eff}$ *versus* ν_{CPMG} are curved for those residues experiencing μs-to-ms time-scale dynamics. Fitting these curves to a two-state model (Carver–Richards) allows the populations (p_A and p_B) and the exchange rates between (k_{ex}) these populations to be extracted. A significant number of residues in free (38 residues) and TCS401-saturated (23 residues) PTP1B exhibited μs-to-ms conformational exchange dynamics. Using an approach that we used previously to analyze p38 mitogen-activated protein kinase dynamics (18), we next identified residues that experience similar exchange dynamics. Briefly, this approach identifies groups of residues with similar fluctuations and thus provides increased statistical significance when evaluating ct-CPMG data.

In free PTP1B, we identified two groups of residues with uniform μs-to-ms conformational exchange dynamics (Table 1). The two clusters showed fast μs exchange dynamics with k_{ex} of 3550–6160 s^{-1}. We identified a small cluster of three residues (group 1) with very fast exchange dynamics (k_{ex} = 6160 ± 360 s^{-1} and p_B = 1.8 ± 1.0%). This cluster exclusively includes residues on the surface of PTP1B, and thus these dynamics likely reflect interactions with bulk solvent (Fig. 3*A*). In contrast, a large cluster (33 residues; group 2) shows exchange dynamics of k_{ex} = 3550 ± 70 s^{-1} and p_B = 3.2 ± 0.4% (p_A open PTP1B form; p_B closed or similar to the PTP1B closed form) and includes residues from most secondary structure elements of PTP1B, including the WPD loop and all other regions of PTP1B that have identified functions in the catalytic activity and allostery of PTP1B. This demonstrates that, in its free form, PTP1B exhibits largely uniform exchange dynamics (Fig. 3*A*).

Comparing our ^{13}C ILV ct-CPMG side-chain relaxation data (38 residues) with previously reported ^{15}N backbone ct-CPMG data (three residues; fit with a k_{ex} = 900 s^{-1} and p_B = 2.3%; Fig. 1*A*) shows similarity (11). Our p_B values are similar to the ones resulting from the ^{15}N backbone ct-CPMG data evaluation (^{13}C ILV ct-CPMG p_B values, 3.2%; ^{15}N backbone ct-CPMG p_B, 2.3%). The populations extracted from our ^{13}C ILV ct-CPMG side chain relaxation data have larger errors, because of the 4-fold increase in k_{ex}, which makes fitting accurate populations more difficult. This 4-fold faster ^{13}C k_{ex}, most likely represents a fast (probably side chain–associated) motion that drives an underlying slower (backbone-associated) motion that was detected in the ^{15}N data. Together, these data show that free PTP1B exhibits mostly fast exchange dynamics and that these can be partitioned into two statistically significant groups. However, the largest, most significant group encompasses most of the protein and highlights the largely uniform exchange behavior throughout free PTP1B.

Active-site binding alters ^{13}C ILV intermediate time-scale dynamics of PTP1B

Next, we evaluated the ^{13}C ILV ct-CPMG side-chain relaxation data for TCS401-saturated (inhibitor bound) PTP1B (WPD loop is closed; helix $\alpha7$ becomes rigidified). The data show a large reduction in the overall exchange dynamics of PTP1B when the active site is occupied. We were able to fit three statistically relevant residue groups (Table 2). Group 1 (3 residues), which exhibits the fastest exchange dynamics (k_{ex} = 2100 ± 240 s^{-1}; p_B = 0.4 ± 0.03%), is a small group and includes only residues in β-strands 8 and 9, which are distant from the PTP1B active site. The exchange dynamics for group 2, which

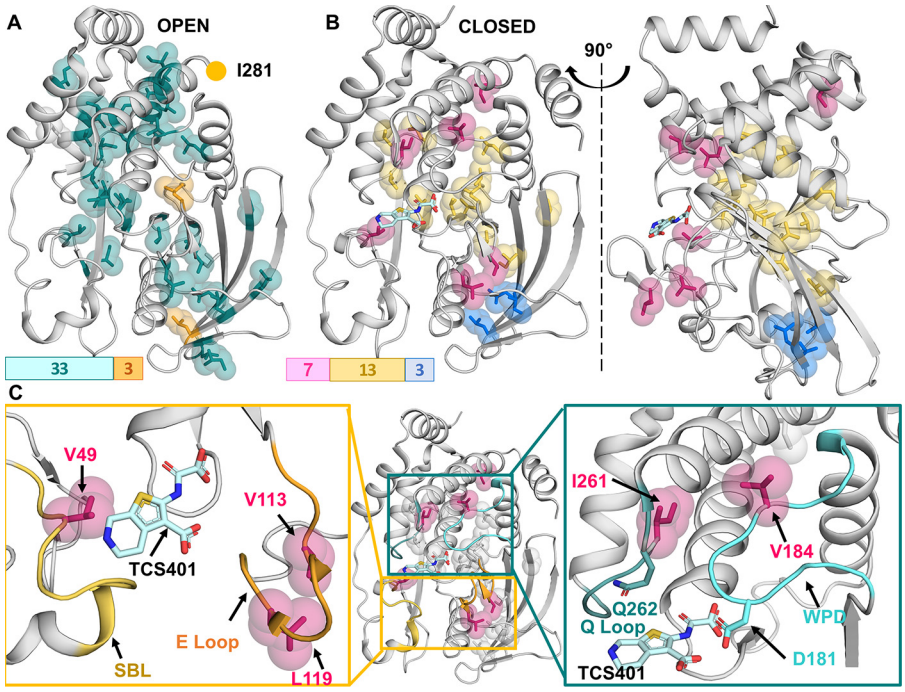

Figure 3. Change in intermediate time-scale ^{13}C ILV relaxation dynamics of PTP1B upon active-site interaction. *A*, PTP1B (open confirmation; PDB 5K9V): group 1 (k_{ex} = 6160 s^{-1}; *orange*); group 2 (k_{ex} = 3550 s^{-1}; *teal*) are shown. *B*, PTP1B (closed confirmation; PDB 5K9W): TCS401 shown as *sticks* (*cyan*). Group 1 (k_{ex} = 2100 s^{-1}; *blue*), group 2 (k_{ex} = 780 s^{-1}; *yellow*), and group 3 (k_{ex} = 550 s^{-1}; *raspberry*) are shown. *C*, detailed analysis of group 3 residues. Residues Val^{49} (SBL), Val^{113}, and Leu^{119} (E loop) are important for substrate recruitment (*yellow box*) and surround the PTP1B active site. Residues Val^{184} (WPD loop) and Ile^{261} (Q loop) are essential for substrate hydrolysis and enzyme regeneration (*teal box*).

Table 2
PTP1B residues in complex with TCS401; specific intermediate exchange group

k_{ex} (s^{-1})	p_B (%)	Residues
550 ± 40	7.8 ± 0.6	Val^{49} (Cγ$_1$), Val^{107} (Cγ$_1$), Val^{113} (Cγ$_1$ and Cγ$_2$), Leu^{119} (Cδ$_1$), Val^{184} (Cγ$_1$), Ile^{261}, Ile^{281}
780 ± 50	2.1 ± 0.1	Leu^{83} (Cδ$_1$), Leu^{110} (Cδ$_1$ and Cδ$_2$), Val^{155} (Cγ$_1$), Leu^{171} (Cδ$_1$), Leu^{195} (Cδ$_1$ and Cδ$_2$), Leu^{204} (Cδ$_1$), Val^{211} (Cγ$_1$), Val^{213} (Cγ$_1$), Leu^{227} (Cδ$_1$ and Cδ$_2$), Leu^{250} (Cδ$_1$ and Cδ$_2$), Leu^{260} (Cδ$_1$), Leu^{272} (Cδ$_1$), Val^{287} (Cγ$_1$)
2100 ± 240	0.40 ± 0.03	Leu^{140} (Cδ$_1$ and Cδ$_2$), Leu^{142} (Cδ$_1$ and Cδ$_2$), Leu^{160} (Cδ$_1$)

is the largest group (13 residues), are significantly slower (k_{ex} = 780 ± 50 s^{-1}; p_B = 2.1 ± 0.2%) and composed of residues surrounding the PTP1B active site and residues present within helices α3/4/6 and β-strands 4/9/10/11. Finally, group 3 (7 residues) exhibits the slowest exchange dynamics (k_{ex} = 550 ± 40 s^{-1}; p_B = 7.8 ± 0.6%). All of these residues belong to structural elements that are critical for PTP1B substrate recruitment and activity, including Val^{184} in the WPD loop (activity), Val^{113} and Leu^{119} of the E loop (substrate recruitment), Val^{49} of the substrate recruitment loop (substrate recruitment), and Ile^{261} of the Q loop (activity; Fig. 3, *B* and *C*). The linked dynamics of these disparate sites in the TCS401-bound state strongly suggest that motions within the active site become synchronized upon binding of inhibitors/substrates.

Only a limited comparison can be made between our ^{13}C ILV ct-CPMG data and the previous ^{15}N backbone ct-CPMG data of closed PTP1B, because the latter analysis is based on a single residue (Ala^{198} in helix α3) and was recorded using a peptide with a nonhydrolyzable tyrosine analog (11). Our data show that the population of the PTP1B open state in TCS401-saturated PTP1B (p_B) is 7.8%, compared with 14% for peptide-saturated PTP1B. This difference in population either reflects the less optimal fit of a single residue or simply reflects the higher affinity of TCS401 for PTP1B *versus* a substrate-like peptide (low μM *versus* high μM to low mM), leading to a higher population of the closed state of PTP1B in our data.

Discussion

Protein dynamics at multiple time scales are essential for protein function and regulation (24–26). NMR spectroscopy is distinctively qualified to report on protein dynamics on multiple time scales, from ps to h. ^{15}N-backbone dynamics, which report on the dynamics of the amide ^{15}N-H^N vector, is the most widely used technique because it has one reporter for each amino acid (except for proline). However, this approach is of limited applicability for larger proteins (≥35 kDa) because their increased overall correlation time τ_c limits sensitivity and resolution. Thus, for these systems the use of ^{13}C-methyl groups for dynamics measurements, especially from ILV residues, has become a routine approach. ^{13}C-H vectors in ILV methyl groups rotate rapidly and thus provide high sensitivity and sharp lines even for very large proteins. Here, we have used ^{13}C ILV relaxation measurements to define the dynamics of PTP1B at different time scales to understand how PTP1B dynamics

correlates with enzymatic function. In particular, although it is well-accepted that multiple structural elements of PTP1B are essential for catalysis (WPD-, SBL-, and Q loops), we set out to determine whether and how these elements are dynamically coordinated, or, alternatively, whether they fulfill their respective functions independently of one another.

Using ^{13}C-methyl group dynamics relaxation experiments, we discovered that PTP1B exhibits dynamics at three distinct time scales. First, and somewhat unexpectedly, we discovered that PTP1B undergoes a distinctive slow motion that allows for the dynamic binding and release of helices $\alpha1'$ and $\alpha2'$ from the core catalytic domain. Among the nonreceptor PTP family, these helices are unique to PTP1B and its most closely related homolog, TCPTP/*PTPN2* (2), suggesting they might have a specific function. If and how these helices contribute to PTP1B (and TCPTP) activity is unknown; however, an intriguing possibility is that the dynamic binding and release of these helices may facilitate substrate recruitment. Second, we confirmed that, in PTP1B, both PTP1B ^{13}C-methyl group side chain fast time-scale dynamics (this work) and ^{15}N backbone fast time-scale dynamics in elements distal from the active site, particularly helix $\alpha7$ (7), are essential for the allosteric control of PTP1B activity. Thus, these data confirm that, in PTP1B, allostery is governed by local fast time-scale dynamics, which modulates intermediate time-scale dynamics that controls the catalytic activity of PTP1B.

Third, we performed ^{13}C ILV ct-CPMG relaxation measurements to measure μs-to-ms exchange dynamics, because this time scale is most often correlated with enzymatic function. In agreement to a previous report, we see a significant 6.5-fold reduction of the WPD loop motion when the active site is occupied (open, k_{ex} = 3550 ± 70 s^{-1}; closed, k_{ex} = 550 ± 40 s^{-1}). However, our comprehensive relaxation data, which reports on dynamics throughout PTP1B (up to 56 distinct residues), significantly expands this observation. Namely, the data show that the functionally critical elements of PTP1B structure fluctuate coherently and distinctly from the rest of the protein when a substrate analog/inhibitor binds the PTP1B active site. This includes residues from the WPD loop, the substrate recruitment E loop, the SBL, and the Q loop. This shows that all catalytically critical residues work in dynamic unity throughout the catalytic cycle of PTP1B.

It is well-recognized that conformational dynamics/plasticity can have an essential role in the catalytic cycle of multiple enzymes. For instance, in cyclophilin A, the observed rate-limiting dynamics reflect coordinated motions across its active site, even in the absence of obvious backbone changes in the corresponding crystal structures (17). However, in the case of PTP1B and other PTPN family members, crystal structures show clearly defined changes in the position of the WPD loop (open/closed) that, in principle, might depict the full range of conformational heterogeneity that allow for the catalytic activity (27). Indeed, similar limited motions that are rate-limiting have been reported for the enzyme triosephosphate isomerase (28). Furthermore, previous results indicated that motions of the PTP1B WPD loop were apparently correlated to the catalytic rate (11), suggesting that this limited model of conformational heterogeneity (WPD loop open/closed) was likely appropriate.

However, further experiments demonstrated that the rate of catalysis of PTP1B is curiously disconnected from the WPD loop's dynamic equilibrium and suggested the involvement of adjacent structural elements in rate-limiting dynamics and thus catalytic activity (7, 10). Indeed, crystallographic evidence from the related protein-tyrosine phosphatase PTPN7 (HePTP) showed coordinated motions of the E loop and WPD loop in response to depletion of a phosphate analog from the binding site (29). Thus, it is likely that coherent/coordinated fluctuations within the active site, either in response to loop opening or in a completely closed state, control catalysis. Our new data add significant support to this latter view. Critically, the greater density of probes provided by uniform ILV labeling allows for the comprehensive observation of dynamic effects throughout the PTP1B active site and shows that all catalytically significant structural elements/loop are engaged in a coherent fluctuation in the presence of an inhibitor, which functioned as a proxy substrate in our analysis. Thus, although the WPD loop mobility is important, it is clearly not the sole contributor to PTP1B dynamics and function at the PTP1B active site.

Taken together, these data suggest that in PTP1B, intermediate dynamics are important for substrate binding and product release, whereas fast dynamics, in elements distal from the chemical reaction, are important for the allosteric control of the overall function of PTP1B. Because these structural features are highly conserved within the PTP family of proteins, it is likely that this pattern of dynamic influence is conserved throughout the PTP family (30). Furthermore, it is likely that sites within these networks can be targeted by new allosteric approaches to modulate PTP function.

Materials and methods

Protein expression

DNA coding the human PTP1B catalytic domain (Uniprot P18031; residues 1–301) was used as previously described (20, 31). For the assignment of ILV residues, the following PTP1B variants were created (QuikChange (Agilent) site-directed mutagenesis): V34A, L37I, L88I, V108A, L172I, L192A, L195A, L199I, L204A, V213A, I219V, L233I, V244I, I261V, L294A, and L299I. Furthermore, also the deletion variant PTP1BΔ7 (PTP1B residues 1–284) was used. For protein expression, plasmid DNA was transformed into *Escherichia coli* BL21 (DE3) RIL cells (Agilent). The cells were grown in M9 minimal medium in the presence of selective antibiotics at 37 °C to an A_{600} of ~0.6, upon amino acid precursors (type depending on labeling scheme) were added. The cells continued to grow at 37 °C until an A_{600} of ~0.8 was reached, and expression was induced by the addition of 1 mM isopropyl β-D-thiogalactopyranoside. Induction proceeded for ~20 h at 18 °C prior to harvesting by centrifugation at 8,000 × *g*. Cell pellets were stored at −80°C until purification. All PTP1B expression in D_2O (22) required careful adaptation (successively in medium containing 25%, 50%, 75%, 90%, and 100% D_2O) to optimize the PTP1B yields.

Multiple labeling schemes were used for different measurements. For the assignment of PTP1B ILV, PTP1B was

expressed with 1 g/liter $^{15}NH_4Cl$, 4 g/liter [^{2}H,^{13}C]-*D*-glucose, [$^{13}C_5$,3-$^2H_1$] 120 mg/liter α-ketoisovaleric acid sodium salt (CDLM 4418) and 60 mg/liter [$^{13}C_4$;3,3-$^2H_2$]α-ketobutyric acid sodium salt (CDLM 4611) in 100% D_2O (scheme 1). To assist in the assignment, PTP1B variants were expressed in M9 medium and labeled with 120 mg/liter [^{13}C]α-ketoisovaleric acid (CDLM 6821) and 60 mg/liter [$^{13}C_2$]α-ketobutyric acid (CDLM 6820) in 100% H_2O (scheme 2). For NOE-based assignment spectra, PTP1B was expressed with 1 g/liter $^{15}NH_4Cl$, 4 g/liter [^{2}H,^{12}C]-*D*-glucose, 120 mg/liter [$^{13}C_5$,3-$^2H_1$]α-ketoisovaleric acid (CDLM 7318) and 60 mg/liter [$^{13}C_4$,3,3-$^2H_2$]α-ketobutyric acid (CDLM 7317) in 100% D_2O (scheme 3). Lastly, for relaxation measurements, PTP1B was expressed with 4 g/liter [^{2}H,^{12}C]-*D*-glucose, 120 mg/liter [3-^{13}C,3-methyl-$^2H_2$, 3,4,4,4-$^2H_4$]α-ketoisovaleric acid (CDLM 7354) and 60 mg/liter [4-^{13}C, 4-$^2H_2$, 3-$^2H_2$]α-ketobutyric acid (CDLM 7353) in 100% D_2O (scheme 4).

Protein purification

PTP1B was purified as previously described into NMR Buffer (10 mM HEPES, pH 7.4, 150 mM NaCl, 5 mM DTT) (7, 20). Purified protein was either used immediately or flash-frozen in liquid nitrogen for storage at −80°C. Samples for NMR dynamics experiments were aliquoted into 550-μl aliquots, flash-frozen in liquid nitrogen, and lyophilized for 24 h. The protein was then resuspended in 550 μl of D_2O. Typical PTP1B protein yields are ~55 mg/liter in D_2O-based M9 minimal medium, and variant yields are ~21–48 mg/liter in M9 minimal medium at 98% purity.

NMR measurements

All PTP1B ^{13}C-methyl ILV assignment NMR measurements were performed using a Bruker Advance Neo 800 MHz NMR spectrometer with a TCI HCN-active z-gradient cryoprobe at 298 K. A 3D (^{13}C,^{13}C,^{1}H)HMCM(CG)CBCA experiment functioned as the initial assignment step using PTP1B produced following scheme 1 (32). A 3D (^{13}C,^{13}C,^{1}H) HSQC-NOESY-HSQC (τ_m = 200 ms) and a 3D (^{13}C,^{15}N,^{1}H)HSQC-NOESY-Heteronuclear multiple quantum coherence (HMQC) (τ_m = 400 ms) spectra were recorded using PTP1B produced following scheme 3. The final concentration of PTP1B for these measurements was 0.35 mM in NMR buffer containing 10% D_2O. All data were processed using NMRPipe (33) or Topspin 4.0.5 and analyzed using NMRFAM-SPARKY (34).

^{13}C-Methyl relaxation NMR measurements ($^{13}CHD_2$) were performed on Bruker Advance Neo 600- and 800-MHz spectrometers equipped with TCI HCN-active z-gradient cryoprobes at 298 K. Data were recorded on ^{2}H,^{12}C,^{15}N-labeled PTP1B with $^{13}CHD_2$-labeled ILV methyl groups (scheme 4), either free or inhibitor/TCS401-saturated at a final protein concentration of 0.25 mM in NMR buffer and 100% D_2O. Sample concentration was tightly monitored to ensure no effect on τ_c and thus $T_{1\rho}$ measurements. TCS401 inhibitor was carefully titrated to achieve full saturation. Upon saturation (chemical shifts of interacting residues stopped changing; usually at 1:3 ratio), additional TCS401 (to 1:6 ratio) was added to ensure that all experiments were performed under fully inhibitor-saturated conditions and thus that the observed CPMG dispersions are independent of ligand on/off exchange events. All relaxation data were recorded as a pseudo-3D in a fully interleaved manner.

T_1 relaxation delays were 20, 500, 1000, 1200, 1400, 1600, 2000, 4000, and 5500 ms (D1 (recycle delay) of 4.5 s; 800 MHz; 1200 and 4000 ms were repeated for measurement error assessment) and 20, 800, 1000, 1200, 1400, 1600, 2000, 2400, 3000, 3200, and 4000 ms (D1 of 4.2 s; 600 MHz; 1200 ms was repeated for measurement error assessment). $T_{1\rho}$ relaxation delays were 5, 30, 50, 60, 90, 100, 120, 150, and 180 (D1 of 2.5 s; 800 MHz; 50 and 150 ms was repeated for measurement error assessment) and 5, 30, 50, 70, 80, 90, 100, 160, 170, and 200 (D1 of 3.2 s; 600 MHz; 70 and 130 ms were repeated for measurement error assessment). The measurement errors between repeat measurements were 2.8% at 18.8T and 2.6% at 14.1T.

ct-CPMG relaxation dispersion experiments were performed at 298 K at two magnetic field strengths (14.1 and 18.8 T). A constant time of 40 ms between ^{15}N refocusing pulses and 10 different delay times corresponding to the following CPMG frequencies 50, 100, 250, 400, 600, 800, 1000, 1200, 1600, and 2000 Hz were used (100 and 800 Hz were repeated for measurement error assessment; which was ~2.8%). D1 was set to 3.2 and 3.8 s for experiments performed on 14.1T and 18.8T magnetic field strengths, respectively.

Relaxation analysis

T_1 and $T_{1\rho}$ values were calculated using NMRviewJ using the peak intensities (jitter function) and exponential decay fitting function. Errors were also determined via relaxation curve fitting. T_2 was extracted from $T_{1\rho}$ by: $R_2 = (R_{1\rho} - R_1\cos^2\beta)/\sin^2\beta$, where β is the effective rotation angle for each ^{15}N nucleus as determined by the strength of the spin-lock field and the chemical shift offset of the nucleus from the spin-lock frequency.

ct-CPMG relaxation dispersion intensity measurements were performed in NMRviewJ (jitter function) and converted to $R_{2\text{eff}}$ by: $R_2eff(\upsilon_{\text{CPMG}}) = (-1/T_{\text{relax}})\ln(I_{\text{CPMG}}/I_0)$. PTP1B residues were fit individually to the Carver–Richards equation for a system in two-state exchange using a Levenberg–Marquardt algorithm. Attempts were then made to fit residues into groups. The quality of the group fit was evaluated using the Bayesian information criterion (BIC) to compare the group fit to the results of the individual fits using $\Delta BIC = BIC_{\text{group}} - BIC_{\text{individual}}$. The more negative the ΔBIC, the better the fit. Groups were refined through several rounds. A residue was kept in a specific group if the BIC was less than −1, and the residuals were randomly distributed.

NMR analysis of TCS401 inhibitor binding

TCS401 was titrated into 0.25 mM PTP1B at molar ratios of 0:1, 0.5:1, 1:1, 2:1, and 3:1 (TCS401:PTP1B). 2D [^{1}H,^{13}C] HSQC spectra were recorded for each titration point. TCS401 was solubilized in d_6-DMSO (25 mM). No chemical shift differences were identified in the PTP1B 2D [^{1}H,^{15}N] Transverse Relaxation Optimized Spectroscopy (TROSY) or 2D [^{1}H,^{13}C]HSQC spectrum upon the addition of d_6-DMSO. Chemical shift perturbations (Δδ) between apo

PTP1B and inhibitor-bound PTP1B spectra were calculated using: $\Delta\delta(ppm) = \sqrt{(\Delta\delta_H)^2 + \left(\frac{\Delta\delta_C}{4}\right)^2}$.

Author contributions—K. R. T., M. W. C., and G. S. K. data curation; K. R. T., M. W. C., and G. S. K. formal analysis; K. R. T. investigation; K. R. T. and M. W. C. methodology; K. R. T., M. W. C., G. S. K., R. P., and W. P. writing-review and editing; M. W. C. software; R. P. and W. P. conceptualization; R. P. and W. P. supervision; R. P. and W. P. funding acquisition; W. P. resources; W. P. writing-original draft; W. P. project administration.

Funding and additional information—This work was supported by the American Diabetes Association Pathway to Stop Diabetes Grant 1-14-ACN-31 (to W. P.) and by National Institutes of Health Grants and R01GM098482 (to R. P.) and T32GM008804 (to K. R. T.). The content is solely the responsibility of the authors and does not necessarily represent the official views of the National Institutes of Health.

Conflict of interest—The authors declare that they have no conflicts of interest with the contents of this article.

Abbreviations—The abbreviations used are: PTP, protein-tyrosine phosphatase; PDB, Protein Data Bank; SBL, substrate-binding loop; ct-CPMG, constant-time Carr–Purcell–Meiboom–Gill; HSQC, heteronuclear single quantum coherence; BIC, Bayesian information criterion.

References

1. Tonks, N. K., Diltz, C. D., and Fischer, E. H. (1988) Purification of the major protein-tyrosine-phosphatases of human placenta. *J. Biol. Chem.* **263,** 6722–6730 Medline
2. Alonso, A., Sasin, J., Bottini, N., Friedberg, I., Friedberg, I., Osterman, A., Godzik, A., Hunter, T., Dixon, J., and Mustelin, T. (2004) Protein tyrosine phosphatases in the human genome. *Cell* **117,** 699–711 CrossRef Medline
3. Feldhammer, M., Uetani, N., Miranda-Saavedra, D., and Tremblay, M. L. (2013) PTP1B: a simple enzyme for a complex world. *Crit. Rev. Biochem. Mol. Biol.* **48,** 430–445 CrossRef Medline
4. Pannifer, A. D., Flint, A. J., Tonks, N. K., and Barford, D. (1998) Visualization of the cysteinyl-phosphate intermediate of a protein-tyrosine phosphatase by x-ray crystallography. *J. Biol. Chem.* **273,** 10454–10462 CrossRef Medline
5. Andersen, J. N., Mortensen, O. H., Peters, G. H., Drake, P. G., Iversen, L. F., Olsen, O. H., Jansen, P. G., Andersen, H. S., Tonks, N. K., and Møller, N. P. (2001) Structural and evolutionary relationships among protein tyrosine phosphatase domains. *Mol. Cell Biol.* **21,** 7117–7136 CrossRef Medline
6. Wiesmann, C., Barr, K. J., Kung, J., Zhu, J., Erlanson, D. A., Shen, W., Fahr, B. J., Zhong, M., Taylor, L., Randal, M., McDowell, R. S., and Hansen, S. K. (2004) Allosteric inhibition of protein tyrosine phosphatase 1B. *Nat. Struct. Mol. Biol.* **11,** 730–737 CrossRef Medline
7. Choy, M. S., Li, Y., Machado, L. E. S. F., Kunze, M. B. A., Connors, C. R., Wei, X., Lindorff-Larsen, K., Page, R., and Peti, W. (2017) Conformational rigidity and protein dynamics at distinct timescales regulate PTP1B activity and allostery. *Mol. Cell* **65,** 644–658.e5 CrossRef Medline
8. Krishnan, N., Koveal, D., Miller, D. H., Xue, B., Akshinthala, S. D., Kragelj, J., Jensen, M. R., Gauss, C.-M., Page, R., Blackledge, M., Muthuswamy, S. K., Peti, W., and Tonks, N. K. (2014) Targeting the disordered C terminus of PTP1B with an allosteric inhibitor. *Nat. Chem. Biol.* **10,** 558–566 CrossRef Medline
9. Keedy, D. A., Hill, Z. B., Biel, J. T., Kang, E., Rettenmaier, T. J., Brandão-Neto, J., Pearce, N. M., von Delft, F., Wells, J. A., and Fraser, J. S. (2018) An expanded allosteric network in PTP1B by multitemperature crystallography, fragment screening, and covalent tethering. *eLife* **7,** e36307 Medline
10. Cui, D. S., Lipchock, J. M., Brookner, D., and Loria, J. P. (2019) Uncovering the molecular interactions in the catalytic loop that modulate the conformational dynamics in protein tyrosine phosphatase 1B. *J. Am. Chem. Soc.* **141,** 12634–12647 CrossRef Medline
11. Whittier, S. K., Hengge, A. C., and Loria, J. P. (2013) Conformational motions regulate phosphoryl transfer in related protein tyrosine phosphatases. *Science* **341,** 899–903 CrossRef Medline
12. Ruschak, A. M., and Kay, L. E. (2010) Methyl groups as probes of supramolecular structure, dynamics and function. *J. Biomol. NMR* **46,** 75–87 CrossRef Medline
13. Tzeng, S.-R., and Kalodimos, C. G. (2011) Protein dynamics and allostery: an NMR view. *Curr. Opin. Struct. Biol.* **21,** 62–67 CrossRef Medline
14. Rosenzweig, R., and Kay, L. E. (2014) Bringing dynamic molecular machines into focus by methyl-TROSY NMR. *Annu. Rev. Biochem.* **83,** 291–315 CrossRef Medline
15. Boehr, D. D., McElheny, D., Dyson, H. J., and Wright, P. E. (2006) The dynamic energy landscape of dihydrofolate reductase catalysis. *Science* **313,** 1638–1642 CrossRef Medline
16. Bhabha, G., Ekiert, D. C., Jennewein, M., Zmasek, C. M., Tuttle, L. M., Kroon, G., Dyson, H. J., Godzik, A., Wilson, I. A., and Wright, P. E. (2013) Divergent evolution of protein conformational dynamics in dihydrofolate reductase. *Nat. Struct. Mol. Biol.* **20,** 1243–1249 CrossRef Medline
17. Otten, R., Liu, L., Kenner, L. R., Clarkson, M. W., Mavor, D., Tawfik, D. S., Kern, D., and Fraser, J. S. (2018) Rescue of conformational dynamics in enzyme catalysis by directed evolution. *Nat. Commun.* **9,** 1314 CrossRef Medline
18. Kumar, G. S., Clarkson, M. W., Kunze, M. B. A., Granata, D., Wand, A. J., Lindorff-Larsen, K., Page, R., and Peti, W. (2018) Dynamic activation and regulation of the mitogen-activated protein kinase p38. *Proc. Natl. Acad. Sci. U.S.A.* **115,** 4655–4660 CrossRef Medline
19. Iverson, D. B., Xiao, Y., Jones, D. N., Eisenmesser, E. Z., and Ahn, N. G. (2020) Activation loop dynamics are coupled to core motions in extracellular signal-regulated kinase-2. *Biochemistry* **59,** 2698–2706 CrossRef
20. Krishnan, N., Krishnan, K., Connors, C. R., Choy, M. S., Page, R., Peti, W., Van Aelst, L., Shea, S. D., and Tonks, N. K. (2015) PTP1B inhibition suggests a therapeutic strategy for Rett syndrome. *J. Clin. Invest.* **125,** 3163–3177 CrossRef Medline
21. Tugarinov, V., and Kay, L. E. (2003) Ile, Leu, and Val methyl assignments of the 723-residue malate synthase G using a new labeling strategy and novel NMR methods. *J. Am. Chem. Soc.* **125,** 13868–13878 CrossRef Medline
22. Peti, W., and Page, R. (2016) NMR spectroscopy to study MAP kinase binding to MAP kinase phosphatases. *Methods Mol. Biol.* **1447,** 181–196 CrossRef Medline
23. Iversen, L. F., Andersen, H. S., Branner, S., Mortensen, S. B., Peters, G. H., Norris, K., Olsen, O. H., Jeppesen, C. B., Lundt, B. F., Ripka, W., Møller, K. B., and Møller, N. P. (2000) Structure-based design of a low molecular weight, nonphosphorus, nonpeptide, and highly selective inhibitor of protein-tyrosine phosphatase 1B. *J. Biol. Chem.* **275,** 10300–10307 CrossRef Medline
24. Tzeng, S.-R., and Kalodimos, C. G. (2012) Protein activity regulation by conformational entropy. *Nature* **488,** 236–240 CrossRef Medline
25. Henzler-Wildman, K. A., Lei, M., Thai, V., Kerns, S. J., Karplus, M., and Kern, D. (2007) A hierarchy of timescales in protein dynamics is linked to enzyme catalysis. *Nature* **450,** 913–916 CrossRef Medline
26. Lisi, G. P., and Loria, J. P. (2016) Using NMR spectroscopy to elucidate the role of molecular motions in enzyme function. *Prog. Nucl. Magn. Reson. Spectrosc.* **92–93,** 1–17 CrossRef Medline
27. Barr, A. J., Ugochukwu, E., Lee, W. H., King, O. N. F., Filippakopoulos, P., Alfano, I., Savitsky, P., Burgess-Brown, N. A., Müller, S., and Knapp, S. (2009) Large-scale structural analysis of the classical human protein tyrosine phosphatome. *Cell* **136,** 352–363 CrossRef Medline
28. Massi, F., Wang, C., and Palmer, A. G. (2006) Solution NMR and computer simulation studies of active site loop motion in triosephosphate isomerase. *Biochemistry* **45,** 10787–10794 CrossRef Medline

29. Critton, D. A., Tautz, L., and Page, R. (2011) Visualizing active-site dynamics in single crystals of HePTP: opening of the WPD loop involves coordinated movement of the E loop. *J. Mol. Biol.* **405,** 619–629 CrossRef Medline
30. Hjortness, M. K., Riccardi, L., Hongdusit, A., Zwart, P. H., Sankaran, B., De Vivo, M., and Fox, J. M. (2018) Evolutionarily conserved allosteric communication in protein tyrosine phosphatases. *Biochemistry* **57,** 6443–6451 CrossRef Medline
31. Peti, W., and Page, R. (2007) Strategies to maximize heterologous protein expression in *Escherichia coli* with minimal cost. *Protein Expr. Purif.* **51,** 1–10 CrossRef Medline
32. Krejcirikova, A., and Tugarinov, V. (2012) 3D-TROSY-based backbone and ILV-methyl resonance assignments of a 319-residue homodimer from a single protein sample. *J. Biomol. NMR* **54,** 135–143 CrossRef Medline
33. Delaglio, F., Grzesiek, S., Vuister, G. W., Zhu, G., Pfeifer, J., and Bax, A. (1995) NMRPipe: a multidimensional spectral processing system based on UNIX pipes. *J. Biomol. NMR* **6,** 277–293 CrossRef Medline
34. Lee, W., Tonelli, M., and Markley, J. L. (2015) NMRFAM-SPARKY: enhanced software for biomolecular NMR spectroscopy. *Bioinformatics* **31,** 1325–1327 CrossRef Medline